ADVANCED MATERIALS

[7] a) R. G. Nuzzo, D. L. Allara, *J. Am. Chem. Soc.* **1983**, *105*, 4481. b) A. Ulman, *An Introduction to Ultrathin Organic Films, from Langmuir–Blodgett to Self-Assembly*, Academic Press, Boston, MA **1991**. c) V. Chechik, R. M. Crooks, C. J. M. Stirling, *Adv. Mater.* **2000**, *12*, 1161.

[8] a) S. Flink, F. C. J. M. van Veggel, D. N. Reinhoudt, *Adv. Mater.* **2000**, *18*, 1315. b) R. N. Nyquist, A. S. Eberhardt, L. A. Silks III, Z. Li, X. Yang, B. I. Swanson, *Langmuir* **2000**, *16*, 1793. c) C.-J. Zhong, M. D. Porter, *Anal. Chem.* **1995**, 709A.

[9] For an example of detection of fluorescence from SAMs on gold see: K. Moteshareі, D. C. Myles, *J. Am. Chem. Soc.* **1998**, *120*, 7328.

[10] a) H. Kuhn, *J. Chem. Phys.* **1970**, *53*, 101. b) O. Inacker, H. Kuhn, *Chem. Phys. Lett.* **1974**, *27*, 317. c) D. S. Karpovich, G. J. Blanchard, *Langmuir* **1996**, *12*, 5522.

[11] For examples of detection of fluorescence from SAMs on glass see: a) N. J. van Veen, S. Flink, M. A. Deij, R. J. M. Egberink, F. C. J. M. van Veggel, D. N. Reinhoudt, *J. Am. Chem. Soc.* **2000**, *122*, 6112. b) M. M. A. Sekar, P. D. Hampton, T. Buranda, G. P. Lopez, *J. Am. Chem. Soc.* **1999**, *121*, 5135. c) S. Flink, F. C. J. M. van Veggel, D. N. Reinhoudt, *Chem. Commun.* **1999**, 2229. d) D. W. J. McCallien, P. L. Burn, H. L. Anderson, *J. Chem. Soc., Perkin Trans. 1* **1997**, 2581. e) D. L. Pilloud, C. C. Moser, K. S. Reddy, P. L. Dutton, *Langmuir* **1998**, *14*, 4809. f) R. A. Bissell, E. Calle, A. P. de Silva, Q. A. N. Gurnaratne, J.-L. Habib-Jiwan, S. L. A. Peiris, R. A. D. D. Rupasinghe, T. K. S. D. Samarasinghe, K. R. A. S. Sandanayake, J. P. Soumimillion, *J. Chem. Soc., Perkin Trans. 2* **1992**, 1559. g) R. A. Potyrailo, R. C. Conrad, A. D. Ellington, G. M. Hieftje, *Anal. Chem.* **1998**, *70*, 3419. h) M. Ayadim, J. L. H. Jiwan, A. P. de Silva, J. P. Soumillion, *Tetrahedron Lett.* **1996**, *37*, 7039.

[12] The monolayers formed by trialkoxysilanes on glass are not strictly "self-assembled", because the coupling to the surface is covalent and not reversible, but it is common to refer to them as SAMs, as they share many characteristics with the "true" self-assembled monolayers. See also: a) J. Sagiv, *J. Am. Chem. Soc.* **1980**, *102*, 92. b) A. Ulman, *Chem. Rev.* **1996**, *70*, 1533. b) V. Chechik, R. M. Crooks, C. J. M. Stirling, *Adv. Mater.* **2000**, *12*, 1161.

[13] D. G. Kurth, T. Bein, *Langmuir* **1993**, *9*, 2965.

[14] Measured monolayer thickness for **MD-1**: 8.4 ± 2 Å. Estimated from CPK models for full surface coverage: 8.5 Å. As expected, a similar thickness was obtained for **MD-2**: 7.9 ± 2 Å. A small thickness increase was found for **MD-3**: 8.92 ± 2 Å (estimated: 9.96 ± 2 Å). Measured monolayer thickness for **MC-1**: 7.2 ± 2 Å (estimated: 8.4 Å). A similar thickness was obtained for **MC-2**: 6.9 ± 2 Å. A small thickness increase was found for **MC-3**: 9.2 ± 2 Å (estimated: 9.9 Å).

[15] Experimental details of contact angle measurements are described in S. Flink, B. A. Boukamp, A. van der Berg, F. C. J. M. van Veggel, D. N. Reinhoudt, *J. Am. Chem. Soc.* **1998**, *120*, 4652.

[16] F. Grieser, P. Thistlethwaite, R. Urquhart, L. K. Patterson, *J. Phys. Chem.* **1987**, *91*, 5286.

[17] R. P. Haugland, in *Handbook of Fluorescent Probes and Research Chemicals* (Ed: M. T. Z. Spence), Molecular Probes, Europe BV, Leiden, The Netherlands **1996**, Ch. 3.

[18] The mass action principle of the system is not ideal probably due to the intrinsic monolayer disorder confirmed by contact angle measurements (see text).

[19] a) M. C. Lonergan, E. J. Severin, B. J. Doleman, S. A. Beaber, R. H. Grubbs, N. S. Lewis, *Chem. Mater.* **1996**, *8*, 2298. b) T. A. Dickinson, D. R. Walt, *Anal. Chem.* **1997**, *69*, 3413.

[20] For sensor arrays, see: a) K. J. Albert, N. S. Lewis, C. L. Schauer, G. A. Sotzing, S. E. Stitzel, T. P. Vaid, D. R. Walt, *Chem. Rev.* **2000**, *100*, 2595. b) J. J. Lavigne, S. Savoy, M. B. Clevenger, J. E. Ritchie, B. McDoniel, S. Yoo, E. V. Anslyn, J. T. MacDewitt, J. B. Shear, D. Neikirk, *J. Am. Chem. Soc.* **1998**, *120*, 6429. For examples of spatially addressable synthesis and epifluorescence analysis, see: a) M. C. Pirrung, *Chem. Rev.* **1997**, *97*, 473. b) P. S. Cremer, T. Yang, *J. Am. Chem. Soc.* **1999**, *121*, 8130.

[21] P. A. Heiney, K. Grüneberg, *Langmuir* **2000**, *16*, 2651.

Formation of a Cobalt Magnetic Dot Array via Block Copolymer Lithography**

By *Joy Y. Cheng*, *C. A. Ross*,* *Vanessa Z.-H. Chan*, *Edwin L. Thomas*, *Rob G. H. Lammertink*, and *G. Julius Vancso*

The fabrication of nanoscale magnetic dot arrays has attracted considerable interest, both for fundamental studies of micromagnetism and for possible applications in high-density magnetic data storage.[1] Single-domain magnetic particles with uniaxial anisotropy are ideal for applications such as patterned recording media, in which each particle stores one bit according to its magnetization direction. To fabricate large area high-density magnetic particle arrays, several lithographic techniques have been used, including interference lithography, X-ray lithography, and nanoimprint lithography.[1–3] Block copolymers which microphase-separate into a monolayer of domains provide a self-assembled template that can also be used for large-area nanolithography.[4,5] The orientation of the block copolymer domains can be controlled by several methods including alignment in a field,[6] or by chemically[7] or topographically[8] patterning the substrate surface. Block-copolymer templates have been used to make nanometer-sized patterns of silicon, silicon nitride, germanium, diamond, and GaAs with periodicity of 20 nm and above.[9–13] Recently, vertical arrays of cobalt nanowires were electroplated through cylindrical holes in a block copolymer template,[14] and Fe nanoporous films were made using a block copolymer mask.[15] In this communication, we demonstrate a process to fabricate an array of cobalt dots from a thin film through successive etching steps, using an organic–organometallic block copolymer as a template. The cobalt dots are small enough to be single-domain magnetic particles, although they do not have uniaxial anisotropy, and have a density of 3×10^{10} dots cm^{-2}. This method is versatile, and can be applied to patterning a wide variety of thin film materials into dot arrays.

There are several important parameters that must be considered when designing a self-assembled block copolymer lithography mask. These parameters include the chemical composition of the different blocks, the stability and compatibility of the block copolymer with the substrate, the morphology of the microphase-separated block copolymer, and the

[*] Prof. C. A. Ross, J. Y. Cheng, Dr. V. Z.-H. Chan, Prof. E. L. Thomas
Department of Materials Science and Engineering
Massachusetts Institute of Technology
Cambridge, MA 02139 (USA)
E-mail: caross@mit.edu

Dr. R. G. H. Lammertink,[+] Prof. G. J. Vancso
Department of Materials Science and Technology of Polymers
MESA Research Institute, University of Twente
P.O. Box 217, NL-7500 AE Enschede (The Netherlands)

[+] Current address: California Institute of Technology, Department of Chemical Engineering 210-41, Pasadena, CA 91125, USA.

[**] The authors gratefully acknowledge the financial support of the MIT Center for Materials Science and Engineering and the University of Twente, and Prof. H. I. Smith for use of the nanofabrication facilities.

  0935-9648/01/1508-1174 $ 17.50+.50/0

length or molar mass of the majority and minority blocks. Lammertink et al. showed that an array of dots can be produced by one-step lithography using a thin film of poly(isoprene-*b*-ferrocenyldimethylsilane) (36 kg/mol PI-*block*-12 kg/mol PFS) which forms PFS cylinders in the bulk phase.[16,17] The synthesis of PFS is done by ring-opening polymerization with anionic initiators.[18–20] Because of the presence of Fe and Si, the organometallic PFS nanodomains are considerably more resistant than the organic PI domains to an O_2 plasma. The etching rate is therefore higher for the PI than for the PFS, and this high selectivity allows a one-step plasma treated PI–PFS block copolymer thin film to be used as a template for nanolithography.[16,17]

However, in the PI–PFS block copolymer, the low glass transition temperature of the PI and its incompatibility with substrate surfaces limits the stability and structural integrity of the nanostructure.[21] Crystallization of the PFS domains can occur at room temperature, at which temperature the PI block is rubbery, resulting in the destruction of the nanodomains. In addition, annealing to improve the phase separation and the domain uniformity can lead to reorganization of the nanodomains and dewetting of the film from the substrate. In the present work, we have used a block copolymer consisting of polystyrene (PS) and PFS (Scheme 1).[22] The PFS domains are more resistant than the PS to etching in an O_2 plasma by a

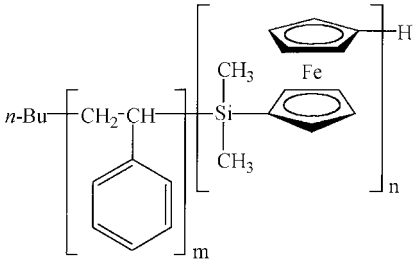

Scheme 1. Chemical structure of poly(styrene-*b*-ferrocenyldimethylsilane) PS-*b*-PFS.

factor of up to 8, enabling the PS matrix to easily be removed. The PS provides improved stability of the nanoscale domain patterns because of its relatively high glass transition temperature, and it is compatible with various substrate surfaces.

We used a PS–PFS block copolymer with 91 kg/mol PS and 21 kg/mol PFS as an example to demonstrate our method of patterning a magnetic thin film. The molar mass of the block copolymer is chosen according to the phase diagram to give 20 vol.-% of PFS spheres embedded in a PS matrix.[22] For fabricating dot arrays, a sphere morphology allows easier processing than a cylindrical morphology, which requires additional boundary conditions such as applied electric fields.[6] When a 2 % solution of this block copolymer is spun onto a substrate and annealed, it forms a 60 nm thick monolayer of close-packed PFS spheres in a PS matrix. The spheres appear to be about 25 nm in diameter and have a periodicity of 50 nm.

The lithographic template is formed by reactive ion etching (RIE) of the block copolymer film in an O_2 plasma.[16,17] This oxidizes the exposed PS matrix and removes it completely, leaving the spherical PFS domains behind. To optimize the process, the effects of the O_2 plasma on the PFS must be understood. The O_2-RIE process consists of both ion-assisted chemical reactions and physical sputtering. The ion-assisted chemical reactions lead to partial oxidation of the PFS domains, in which the silicon and iron in the PFS form a silicon–iron oxide. This effect was quantified by using X-ray photoelectron spectroscopy (XPS) to determine the surface composition and chemical states of a PFS homopolymer etched in O_2 plasma. An oxygen 1s peak appears in the oxidized PFS, and the binding energy of the silicon 2p and iron 2p peaks increases, indicating that the PFS homopolymer is partially converted to an iron–silicon oxide containing carbon[17] (Table 1).

Table 1. At.-% composition of the PFS homopolymer after various 2 min RIE treatments, from XPS.

Elements	Unetched PFS	60V O_2-RIE	200V O_2-RIE	60V O_2-RIE then 150V CHF_3-RIE
C	85.7	29.3	18.9	48
O	0.6	46.8	53.0	6
Si	6.0	8.5	10.9	3
Fe	7.7	15.4	17.2	4
F	-	-	-	39

In the block copolymer, this iron–silicon oxide is believed to form a protective layer around the PFS domains, reducing their etch rate during the O_2-RIE process, and leading to good topographic contrast in the oxidized PS–PFS block copolymer. The key to utilizing such a film as a lithographic mask is to remove the PS matrix to leave PFS features with a large aspect ratio (height/width) and straight sidewalls. This can be optimized by choice of etching time and bias voltage.

First, the endpoint of the block copolymer O_2-etching process was determined from scanning electron microscopy (SEM) images and from measurements of the refractive index of the film using ellipsometry. Figure 1a shows a cross-sectional SEM image of the partially etched PS–PFS block copolymer film. It appears that about half the thickness of the PS has been removed, and oxidized PFS posts can be seen emerging from the remaining PS matrix. The original size and spacing of the close-packed spherical nanostructure is preserved. There was a good correlation between the endpoint detected from SEM and from ellipsometry. The refractive index decreased linearly with etching time until the PS had been etched down to the substrate, at which point the refractive index stopped changing. PS endpoint detection allows etching of the PFS domains to be minimized, thus raising the aspect ratio of the posts.

The shape and uniformity of the remaining PFS features were optimized by adjusting the direct current (DC) bias used during RIE. In the O_2-RIE process, there is a competition between oxide formation by the ion-assisted chemical reaction and removal of material through physical sputtering,

  0935-9648/01/1508-1175 $ 17.50+.50/0

ADVANCED MATERIALS

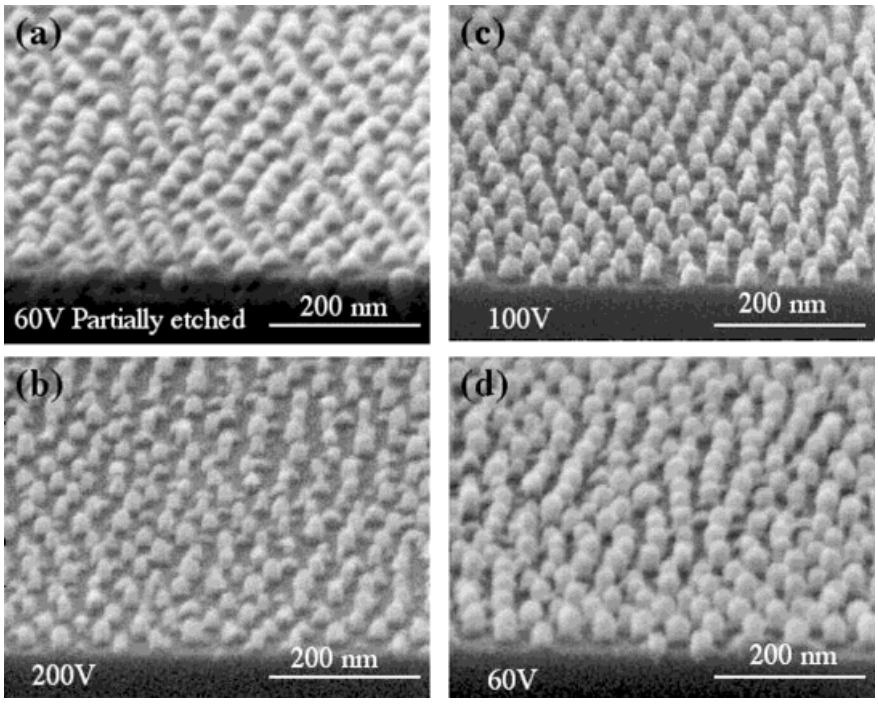

Fig. 1. Tilted SEM images of O_2-RIE etched PS–PFS copolymer. a) PS-*b*-PFS etched partway through the PS. A layer of PS is still left on the substrate, with PFS domains protruding. b) PS-*b*-PFS etched completely through the PS matrix, using 200 V DC bias. c) PS-*b*-PFS etched completely, using 100 V DC bias. d) PS-*b*-PFS etched completely, using 60 V DC bias.

which leads to a change both in the morphology of the remaining PFS features, and in the relative etch rates of the PS and PFS, as a function of DC bias. At higher bias there was a decrease in the etching selectivity between PS and PFS. 60 V DC bias gave the greatest difference in etch rates (PS/PFS = 8:1), 100 V DC bias gives less selectivity (5:1) and 200 V DC bias gives the least selectivity (2:1). This result can be explained by comparing the effects of bias on both etching and oxidation of the PFS. From XPS measurements on the homopolymer (Table 1), it appears that under higher bias, ion-assisted oxidation is faster and more of the PFS is converted into the non-volatile iron–silicon oxide. This would by itself reduce the removal rate of the PFS. However, under higher bias, physical sputtering becomes the dominant mechanism for material removal, leading to higher etch rates and a decrease in the selectivity between PS and PFS.

The SEM images of Figure 1b–d show the nanostructures formed under different bias conditions. At 200 V DC bias, tapered features with an average base diameter of 22 nm are formed (Fig. 1b). At 100 V bias, cylindrical features with straight sidewalls were formed, with an average diameter of 27 nm (Fig. 1c). At 60 V, the features have straight sidewalls and improved uniformity, and an average diameter of 33 nm. Therefore, relatively low bias conditions (60 V) must be used in order to obtain anisotropic etching to preserve the straight sidewalls of the features, while maintaining a high selectivity between the PS and PFS domains. Similar trends have been observed in surface image resist systems, where the silylation layer is destroyed by a high power flux.[23] This optimization of the O_2-RIE process enables us to make lithographic masks with arrays of posts of 30–40 nm in height and 20–30 nm in diameter from a single spin-coated block copolymer film. In addition to changing the etching conditions, the feature size can be adjusted by changing the molar mass of the block copolymer.

The next step is to transfer the template pattern into a magnetic film using intermediate masking layers. Materials such as iron, nickel, and cobalt cannot be etched using an RIE process because they do not form volatile products.[24] Hence, to transfer the pattern from the template into the magnetic layer, we developed a multilayer scheme, which uses a combination of reactive ion etching and ion beam etching. Figure 2 summarizes the materials, procedures and intermediate nanostructures for this process. The multilayer consists of electron-beam evaporated chromium, cobalt, tungsten, then silica, with each layer 5–30 nm thick. (The chromium

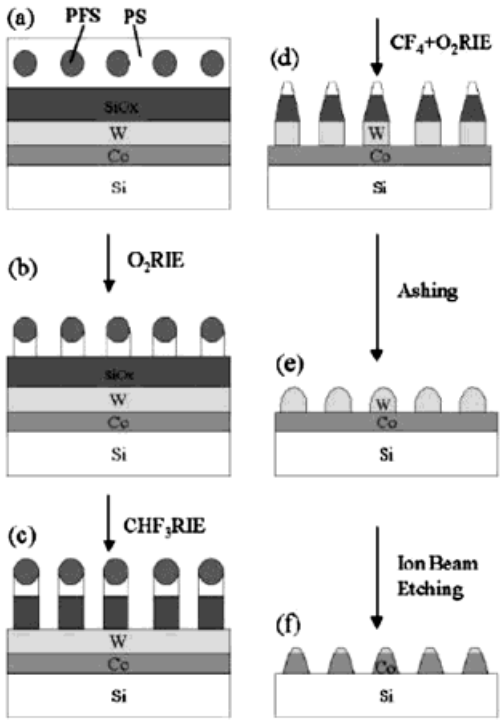

Fig. 2. Fabrication process of the cobalt dot array via block copolymer lithography. a) A block copolymer thin film on a multilayer of silica, tungsten, and cobalt. b) The block copolymer lithographic mask is formed through O_2-RIE process. The PFS domains are partly oxidized. c) The silica film is patterned using CHF_3-RIE. d) The tungsten hard mask is patterned using CF_4 + O_2-RIE. e) Removal of silica and residual polymer by high pressure CHF_3-RIE. f) The cobalt dot array is formed using ion beam etching.

  0935-9648/01/1508-1176 $ 17.50+.50/0

serves as an adhesion layer for the cobalt.) The pattern in the block copolymer template is transferred sequentially through the silica, then the tungsten, then the cobalt. Tungsten was chosen to provide a hard-mask for ion-beam etching of the cobalt. The silica layer was introduced to improve the pattern transfer from the block copolymer template into the tungsten. The silica layer forms a robust template, which can be used to pattern a variety of materials including tungsten, other metals, or other polymeric layers.

Figure 3a is an SEM image of the lithographic mask (etched polymer film) on top of the multilayer stack, which corresponds to the schematic structure in Figure 2b. A CHF_3 RIE was used to transfer the pattern from the lithographic mask to the silica. XPS showed that after etching a PFS homopolymer with O_2 then CHF_3, the surface becomes richer in fluorine (Table 1), indicating that the CHF_3 forms a passivation layer on the oxidized PFS. There is good RIE selectivity between the oxidized PFS lithographic mask and the silica using CHF_3 gas.[25] The selectivity is SiO_2/PFS = 10:1, which ensures the preservation of the pattern during etching. The result of etching a 30 nm thick silica layer with CHF_3 RIE is shown in Figure 3b. Tall pillars of silicon oxide capped with oxidized PFS are seen, with average height of 60 nm, corresponding to the schematic structure in Figure 2c. The high aspect ratio of these features should be noted.

A CF_4 and O_2 gas mixture was subsequently used to etch through the tungsten layer using the silica as a mask. The selectivity is W/SiO_2 = 3:1. The 30 nm thick silica mask was used successfully to pattern a 15 nm thick tungsten film, preserving the lateral dimensions of the features. After patterning the tungsten, the silica and any residual oxidized PFS were removed by an ashing process with a high pressure CHF_3 plasma (Fig. 2e). Figure 3c shows a 15 nm thick patterned tungsten film on top of a cobalt layer after removal of the silica and oxidized PFS caps.

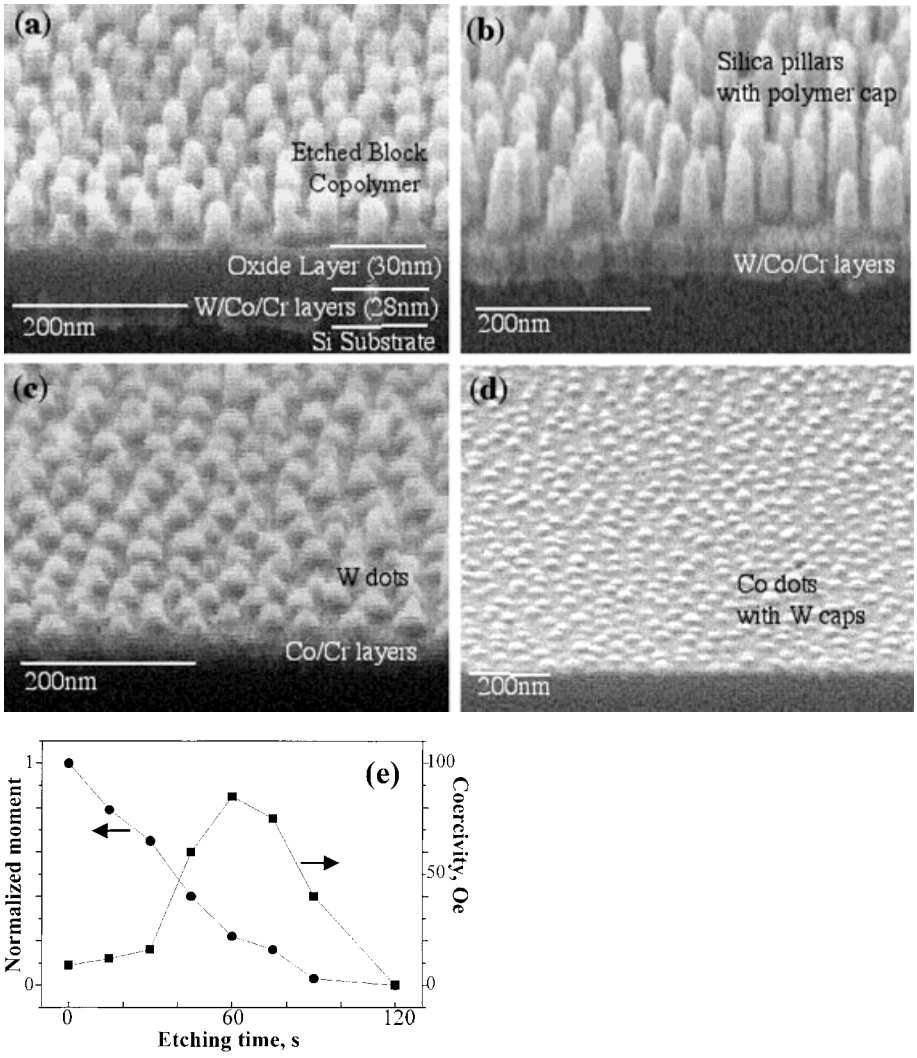

Fig. 3. Tilted SEM images of the intermediate stages of lithographic processing. a) An O_2-RIE treated block copolymer thin film on a multilayer of silica, the metallic films, and the silicon substrate. b) Pillars of silicon oxide capped with oxidized PFS after CHF_3-RIE. c) Patterned tungsten film on top of a cobalt layer after removing the silica and residual polymer cap. d) W-capped cobalt dot array produced by block copolymer lithography (note different magnification). e) Saturation magnetization and coercivity as a function of ion beam etching time.

Finally, ion beam etching, a purely physical sputtering process, was used to pattern the 8 nm thick cobalt, with the 15 nm thick tungsten dots serving as a hard mask (Fig. 3d). The sputtering rate is related to energy transfer from the bombarding gas ions to the substrate material: if there is a large difference in atomic mass, energy transfer will be minimized and the film will be etched slowly.[26] Because of its high atomic mass and process compatibility with silica, W (M = 184 amu) is a good choice as a hard mask for patterning Co (M = 60 amu) employing Ar^+. At 500 eV argon ion energy, the cobalt is removed 1.4 times faster than the tungsten.[22] If desired, the remaining tungsten mask can be removed from the cobalt by RIE.

Figure 3e shows how coercivity and saturation magnetization of the cobalt thin film change with ion-beam etching time. The saturation magnetization, which is proportional to the volume of cobalt, decreases linearly with time during the first minute of etching as the cobalt directly exposed to the ion beam is removed. Further etching results in a slower decrease in magnetization with time as the diameter of the tungsten-capped cobalt fea-

  0935-9648/01/1508-1177 $ 17.50+.50/0

ADVANCED MATERIALS

tures is decreased. The end-point of the etching is approximately 60 s, at which a discrete cobalt dot array is formed. The coercivity increases during the first minute of the etching process as domain wall motion is impeded by the corrugations in the cobalt film created by the sputtering process. The coercivity reaches a maximum at the point that discrete cobalt particles are formed, and then decreases as the volume of the cobalt particles decreases. The cobalt dots at the end point of etching have diameters of 20 nm, which is equal to three times the magnetic exchange length of 7 nm in cobalt. At this size, micromagnetic modeling predicts that the dots should be single-domain particles, because the particles are too small to support a domain wall.[27] This means that the magnetization is approximately uniform within these cobalt particles (with some deviations at the edges or corners). The particles presented here have an easy in-plane magnetization direction. An out-of-plane easy axis, which is preferable for data storage, could be introduced by increasing the aspect ratio, by orienting the cobalt *c*-axes out of plane or by patterning a multilayer film such as Co/Pt or Co/Pd with perpendicular anisotropy.

In conclusion, single-domain cobalt dot arrays have been fabricated using self-assembled block copolymer lithography. There are several advantages to the fabrication process that we have developed. The process allows high density arrays of dots to be fabricated: the magnetic particle density illustrated here is 30 Gparticles cm^{-2}. The process can pattern large areas, such as 10 cm diameter wafers. The process can be applied very generally to pattern a variety of thin-film materials into dot arrays. In addition, particle sizes and spacings can be controlled through the choice of the block copolymer template and etching conditions. Therefore, magnetic properties such as coercivity, anisotropy, magnetostatic interactions, and thermal stability are adjustable in this fabrication system through both the geometric parameters of the particle array and the composition and growth of the magnetic thin film. We are currently characterizing the magnetic behavior of various dot arrays, and pursuing in-plane ordering of the block copolymer nanodomains.

Experimental

Poly(styrene-*block*-ferrocenyldimethylsilane) (PS-*b*-PFS) copolymer was synthesized by sequential anionic polymerization. Polymerization of styrene in ethylbenzene was initiated by *n*-butyllithium. After the styrene block formation was complete, 1,1′-dimethylsilylferrocenophane and tetrahydrofuran (THF) were added for polymerization of the ferrocenyldimethylsilane block. The block copolymer was precipitated in methanol and characterized with gel permeation chromatography (GPC). Its polydispersity was less than 1.1. The block copolymer was spin-coated as a 1–3 wt.-% PS-*b*-PFS or PFS solution in toluene to form 40–80 nm thick films. The thin films of W, SiO_2, Co, and Cr were deposited using an Airco Temescal BJD 1800 electron-beam evaporator.

All reactive ion etching was performed on a Plasma Therm Model 790. O_2-RIE at 5 mtorr and various bias conditions transformed the block copolymer film into a lithographic mask. CHF_3-RIE performed at 150 V DC bias and 15 mtorr had the best anisotropy and selectivity for etching SiO_2. A mixture of 85 % CF_4 and 15 % O_2 with a total pressure of 15 mtorr and 70 V DC bias was used to etch the W. The SiO_2 and residual PFS were removed by CHF_3-RIE at 100 V DC bias and 25 mtorr. Co etching was performed on an Ion Tech ion beam etcher, using 500 V Ar^+ at 0.5 mA cm^{-2} and 0.3 mtorr.

PFS thin films were characterized with a Kratos Axis ultra X-ray photoelectron spectrometer using an Al source with input power of 225 W (15 kV and 15 mA). Elemental concentrations were determined from the relative peak areas integrated numerically. High resolution SEM was performed on specimens coated with 1–2 nm gold using a LEO 982 Gemini SEM with a field emission source at 5 kV to 15 kV. The magnetic properties of the ion beam-etched Co films were studied with a Princeton MicroMag 2900 alternating gradient magnetometer using a gradient field of 1 Oe.

Received: December 28, 2000
Final version: March 13, 2001

[1] C. A. Ross, H. I. Smith, T. Savas, M. Schattenburg, M. Farhoud, M. Hwang, M. Walsh, M. Abraham, R. Ram, *J. Vac. Sci. Technol. B* **1999**, *17*, 3168.
[2] F. Rousseaux, D. Decanini, F. Carcenac, E. Cambril, M. F. Ravet, C. Chappert, N. Bardou, B. Bartenlian, P. Veillet, *J. Vac. Sci. Technol. B* **1995**, *13*, 2787.
[3] W. Wu, B. Cui, X. Y. Sun, W. Zhang, L. Zhuang, L. S. Kong, S. Y. Chou, *J. Vac. Sci. Technol. B* **1998**, *16*, 3825.
[4] P. Mansky, P. Chaikin, E. L. Thomas, *J. Mater. Sci.* **1995**, *30*, 1987.
[5] T. Thurn-Albrecht, R. Steiner, J. deRouchey, C. M. Stafford, E. Huang, M. Bal, M. T. Tuominen, C. J. Hawker, T. P. Russell, *Adv. Mater.* **2000**, *12*, 787.
[6] T. L. Morkved, M. Lu, A. M. Urbas, E. E. Ehrichs, H. M. Jaeger, P. Mansky, T. P. Russell, *Science* **1996**, *273*, 931.
[7] R. D. Peters, X. M. Yang, Q. Wang, J. J. de Pablo, P. F. Nealy, *J. Vac. Sci. Technol. B* **2000**, *18*, 3530.
[8] R. A. Segalman, H. Yokohama, E. J. Kramer, *APS Meeting*, Minneapolis, MN, March 20–24, **2000**.
[9] M. Park, C. Harrison, P. M. Chaikin, R. A. Register, D. H. Adamson, *Science* **1997**, *276*, 1401.
[10] C. Harrison, M. Park, P. M. Chaikin, R. A. Register, D. H. Adamson, *J. Vac. Sci. Technol. B* **1998**, *16*, 544.
[11] R. R. Li, P. D. Dapkus, M. E. Thompson, W. G. Jeong, C. Harrison, P. M. Chaikin, R. A. Register, D. H. Adamson, *Appl. Phys. Lett.* **2000**, *76*, 1689.
[12] J. P. Spatz, T. Herzog, S. Mossmer, P. Ziemann, M. Moller, *Adv. Mater.* **1999**, *11*, 149.
[13] B. Koslowski, S. Strobel, T. Herzog, H. G. Boyen, R. Notz, P. Ziemann, J. P. Spatz, M. Moller, *J. Appl. Phys.* **2000**, *87*, 7533.
[14] T. Thurn-Albrecht, J. Schotter, G. A. Kastle, N. Emley, T. Shibauchi, L. Krusin-Elbaum, K. Guarini, C. T. Black, M. T. Tuominen, T. P. Russell, *Science* **2000**, *290*, 2126.
[15] K. Liu, S. M. Baker, M. T. Tuominen, T. P. Russell, I. K. Schuller, *Phys. Rev. B* **2001**, *6305*, 060403.
[16] R. G. H. Lammertink, M. A. Hempenius, J. E. van den Enk, V. Z.-H. Chan, E. L. Thomas, G. J. Vancso, *Adv. Mater.* **2000**, *12*, 98.
[17] R. G. H. Lammertink, M. A. Hempenius, V. Z.-H. Chan, E. L. Thomas, G. J. Vancso, *Chem. Mater.* **2001**, *13*, 429.
[18] D. A. Foucher, B. Z. Tang, I. Manners, *J. Am. Chem. Soc.* **1992**, *114*, 6246.
[19] Y. Ni, R. Rulkens, I. Manners, *J. Am. Chem. Soc.* **1996**, *118*, 4102.
[20] I. Manners, *Chem. Commun.* **1999**, 857.
[21] R. G. H. Lammertink, M. A. Hempenius, G. J. Vancso, *Langmuir* **2000**, *16*, 6245.
[22] R. G. H. Lammertink, M. A. Hempenius, E. L. Thomas, G. J. Vancso, *J. Polym. Sci., Part B: Polym. Phys.* **1999**, *37*, 1009.
[23] J. Munoz, C. Dominguez, *J. Vac. Sci. Technol. B* **1995**, *13*, 2179.
[24] M. E. Walsh, Y. Hao, C. A. Ross, H. I. Smith, *J. Vac. Sci. Technol. B* **2000**, *18*, 3530.
[25] D. L. Flamm, G. K. Herb, *Plasma Etching, An Introduction*, Academic Press, New York **1988**.
[26] M. Ohring, *The Materials Science of Thin Films*, Academic Press, New York **1992**.
[27] C. A. Ross, M. Farhoud, M. Hwang, H. I. Smith, M. Redjdal, F. B. Humphrey, *J. Appl. Phys.* **2001**, *89*, 1310.

  0935-9648/01/1508-1178 $ 17.50+.50/0